Two coupled, driven Ising spin systems working as an engine

Debarshi Basu,[1] Joydip Nandi,[1] A. M. Jayannavar,[2,3] and Rahul Marathe[1,*]
[1]*Department of Physics, Indian Institute of Technology, Delhi, Hauz Khas 110016, New Delhi, India*
[2]*Institute of Physics, Sachivalaya Marg, Bhubaneshwar 751005, Odhisha, India*
[3]*Homi Bhabha National Institute, Training School Complex, Anushakti Nagar, Mumbai 400085, India*
(Received 3 October 2016; published 12 May 2017)

Miniaturized heat engines constitute a fascinating field of current research. Many theoretical and experimental studies are being conducted that involve colloidal particles in harmonic traps as well as bacterial baths acting like thermal baths. These systems are micron-sized and are subjected to large thermal fluctuations. Hence, for these systems average thermodynamic quantities, such as work done, heat exchanged, and efficiency, lose meaning unless otherwise supported by their full probability distributions. Earlier studies on microengines are concerned with applying Carnot or Stirling engine protocols to miniaturized systems, where system undergoes typical two isothermal and two adiabatic changes. Unlike these models we study a prototype system of two classical Ising spins driven by time-dependent, phase-different, external magnetic fields. These spins are *simultaneously* in contact with two heat reservoirs at different temperatures for the full duration of the driving protocol. Performance of the model as an engine or a refrigerator depends only on a single parameter, namely the phase between two external drivings. We study this system in terms of fluctuations in efficiency and coefficient of performance (COP). We find full distributions of these quantities numerically and study the tails of these distributions. We also study reliability of the engine. We find the fluctuations dominate mean values of efficiency and COP, and their probability distributions are broad with power law tails.

DOI: 10.1103/PhysRevE.95.052123

I. INTRODUCTION

After Feynman's theoretical construction of his famous Ratchet and Pawl machine in Ref. [1], due to advancement in nanoscience, it is now possible to realize miniaturized engines experimentally [2–5]. Many of the experiments are based on theoretical predictions, namely the fluctuation theorems that put bounds on thermodynamic quantities of interest, like efficiency of the engines [6,7]. For thermodynamic engines, such as Carnot or Stirling, the fluctuations are usually ignored and most of the physics is obtained from average values of work and heat [8]. These notions, however, fail in the case of microscopic engines. Microengines behave differently and the main reason behind this odd behavior are the *loud* thermal fluctuations. These thermal fluctuations cause energy exchanges of the order of k_BT, where k_B is the Boltzmann constant and T is the ambient temperature. For small systems one can thus not just rely on mean values of work and heat or, as a matter of fact, any thermodynamic quantity, but one has to look at full probability distributions. To deal with such systems, one needs to use the framework of stochastic thermodynamics [9–11]. Many studies on such small-scale engines have shown that fluctuations in thermodynamic quantities dominate over mean values even in the quasistatic limit [12–19]. Many studies have also looked at full distributions of efficiency [13,14] and also the large deviation functions [20]. Models with feedback control both instantaneous and delayed have also been investigated [21–24]. Most of the earlier studies, both theoretical and experimental, were based on applying the thermodynamic engine protocols, such as Carnot or Stirling, to a colloidal particle placed in an harmonic trap. The trap strength is then modified time dependently to mimic isothermal expansion, compression and adiabatic expansion, compression steps [2,3,13,14]. We would like to point out that there are, in fact, no detailed studies that deal with fluctuations of thermodynamic quantities for externally driven systems that are simultaneously in contact with several heat baths. These systems show many features not seen in earlier studied models.

In this work, we have studied a model of classical heat engine and a pump where two Ising spins are independently kept in contact with two heat baths at different temperatures. These spins are externally driven by time-dependent magnetic fields with a phase difference [25]; see Fig. 1. During full driving, protocol system is never isolated from the heat baths. Interestingly the phase difference is the only parameter that decides whether system works as a heat engine or a refrigerator. Performance of this model in terms of average heat currents has been studied in Ref. [25]. In this paper, we analyze this model in terms of the following:

(1) rich features this model exhibits in phase diagrams of engine and pump performance;

(2) fluctuations in efficiency, COP, and their probability distributions, including power-law tails;

(3) behavior of work, heat, efficiency, and power in quasistatic limit;

(4) reliability of the model to work either as an engine or a refrigerator.

II. MODEL

We consider a model of two classical Ising spins with interaction energy J, driven by time-dependent external magnetic fields $h_1(t) = h_0\cos(\omega t)$ and $h_2(t) = h_0\cos(\omega t + \phi)$, where ϕ is the phase difference and ω the driving frequency, as shown in Fig. 1. The Hamiltonian for this system is

*maratherahul@physics.iitd.ac.in

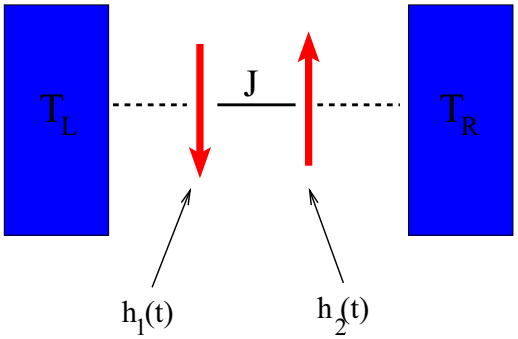

FIG. 1. Cartoon of the model discussed in the text.

written as

$$\mathcal{H} = -J\sigma_1\sigma_2 - h_1(t)\sigma_1 - h_2(t)\sigma_2, \ \ \sigma_{1,2} = \pm 1. \tag{1}$$

Left and right spins are in contact with heat baths at temperature T_L and T_R, respectively. Interaction of spins with the respective heat baths is modeled by Glauber dynamics [26]. We define heat currents coming from left (right) baths $\dot{Q}_L$ ($\dot{Q}_R$) and work done on left (right) spin $\dot{W}_L$ ($\dot{W}_R$) to be positive. The total work done is nothing but $\dot{W} = \dot{W}_L + \dot{W}_R$. If $P(\sigma_1,\sigma_2,t)$ represents the probability to have spins in state $\{\sigma_1,\sigma_2\}$ at time t, then the heat-exchange rates can be written as

$$\begin{aligned}
\dot{Q}_L &= \sum_{\sigma_1,\sigma_2} P(\sigma_1,\sigma_2,t) r^L_{\sigma_1,\sigma_2} \Delta E_1(\sigma_1,\sigma_2),\\
\dot{Q}_R &= \sum_{\sigma_1,\sigma_2} P(\sigma_1,\sigma_2,t) r^R_{\sigma_1,\sigma_2} \Delta E_2(\sigma_1,\sigma_2),\\
\dot{W}_L &= -\langle\sigma_1\rangle\dot{h}_1(t) = -\dot{h}_1(t)\sum_{\sigma_1,\sigma_2}\sigma_1 P(\sigma_1,\sigma_2,t),\\
\dot{W}_R &= -\langle\sigma_2\rangle\dot{h}_2(t) = -\dot{h}_2(t)\sum_{\sigma_1,\sigma_2}\sigma_2 P(\sigma_1,\sigma_2,t),
\end{aligned} \tag{2}$$

where the modified Glauber spin flip rates to compensate for two heat reservoirs are given by

$$r^{L,R}_{\sigma_1,\sigma_2} = r(1-\gamma_{L,R}\sigma_1\sigma_2)(1-\delta_{L,R}\sigma_{1,2}), \tag{3}$$

with

$$\begin{aligned}
\gamma_{L,R} &= \tanh(J/k_B T_{L,R}),\\
\delta_{L,R} &= \tanh(h_{1,2}/k_B T_{L,R}),
\end{aligned} \tag{4}$$

where r is a rate constant. The energy changes associated with left or right spin flips are given by

$$\begin{aligned}
\Delta E_1 &= 2[J\sigma_1\sigma_2 + h_1(t)\sigma_1],\\
\Delta E_2 &= 2[J\sigma_1\sigma_2 + h_2(t)\sigma_2].
\end{aligned} \tag{5}$$

Expressions in Eq. (2) can be easily obtained from the master equation satisfied by $P(\sigma_1,\sigma_2,t)$; see Ref. [25] for details. It is easy to show that the average energy $U = \langle\mathcal{H}\rangle = \sum_{\sigma_1,\sigma_2}\mathcal{H}(\sigma_1,\sigma_2)P(\sigma_1,\sigma_2,t)$ and $\dot{U} = \dot{Q}_L + \dot{Q}_R + \dot{W}_L + \dot{W}_R$ from the above expressions. Since external driving is time dependent, after a transient period probability $P(\sigma_1,\sigma_2,t)$ attains a time periodic state that is independent of the initial state. We also define time-averaged heat and work currents, namely,

$$\begin{aligned}
\langle\dot{q}_{L,R}\rangle &= 1/\tau\int_0^\tau \dot{Q}_{L,R}dt,\\
\langle\dot{w}\rangle &= 1/\tau\int_0^\tau \dot{W}dt,
\end{aligned} \tag{6}$$

where $\tau = 2\pi/\omega$ is the time period of the external driving.

Once these definitions are set, for $T_L \geqslant T_R$, we define stochastic efficiency ϵ and stochastic coefficient of performance (COP) η as

$$\epsilon = \frac{\dot{w}}{-\dot{q}_L}, \ \eta = \frac{\dot{q}_R}{\dot{w}}. \tag{7}$$

We note that due to large thermal fluctuations, two efficiencies

$$\bar{\epsilon} = \frac{\langle\dot{w}\rangle}{\langle-\dot{q}_L\rangle} \text{ and } \langle\epsilon\rangle = \left\langle\frac{\dot{w}}{-\dot{q}_L}\right\rangle,$$

are in general not equal that is $\langle\epsilon\rangle \neq \bar{\epsilon}$ similarly $\langle\eta\rangle \neq \bar{\eta}$. For completeness we reproduce results from Ref. [25] to show how the phase ϕ and time period τ determine the engine or pump behavior. In Figs. 2(a) and 2(b), we plot $\langle\dot{w}\rangle$, $\langle\dot{q}_L\rangle$, and $\langle\dot{q}_R\rangle$ as a function of the phase ϕ for engine and pump mode of operation, respectively. In Fig. 2(a), for all values of ϕ the heats $\langle\dot{q}_L\rangle > 0$, $\langle\dot{q}_R\rangle < 0$ but for a narrow range $\pi/2 \leqslant \phi \leqslant \pi$ work done $\langle\dot{w}\rangle < 0$. In this narrow range, work is extracted from the system, hence the device works as an engine. It can be seen that for parameters $T_L = 1.0$, $T_R = 0.1$, $J = 1.0$, $h_0 = 0.25$, and $\tau = 190$, at $\phi = 0.7\pi$ maximum work is extracted. We refer to this set of parameter values as optimal parameters for engine mode of operation throughout the manuscript. Similarly, in Fig. 2(b), for all values of ϕ work done $\langle\dot{w}\rangle > 0$, but the heats $\langle\dot{q}_L\rangle$ and $\langle\dot{q}_R\rangle$ take positive and negative values alternately. For a narrow strip $\pi/2 \leqslant \phi \leqslant \pi$, $\langle\dot{q}_L\rangle < 0$ and $\langle\dot{q}_R\rangle > 0$, thus the system works like a pump, transferring heat from the right bath to the left. For parameters $T_L = 0.5$, $T_R = 0.5$, $J = 1.0$, $h_0 = 0.25$, and $\tau = 225$, at about $\phi = 0.7\pi$ maximum pumping of heat happens. Thus, we refer to these parameter values as optimal parameters for refrigerator-pump mode of operation throughout the manuscript. Similar results, as in Fig. 2(b) are obtained if the right bath is slightly colder showing one can transfer heat from colder to hotter bath working as a refrigerator; see Ref. [25].

The average values of heats and work done can easily be obtained by solving the master equation numerically [25]. But to study fluctuations and distributions of these quantities, we have to rely on Monte Carlo simulations, which we now describe.

III. SIMULATIONS

To study the dynamics of the system and for evaluating different heat currents, we perform Monte Carlo simulations. We discretize the magnetic field sweep, which consists of $\sim 10^4$ time steps such that each time step $dt = \tau/10^4$ with $\tau = 2\pi/\omega$, where τ is the time period of external driving. We also fix the Boltzmann constant $k_B = 1$, the interaction energy $J = 1.0$, and the rate constant $r = 0.5$. Simulation follows usual Monte Carlo steps in which first or second spin is chosen at random. At each discrete time step, only one spin may flip.

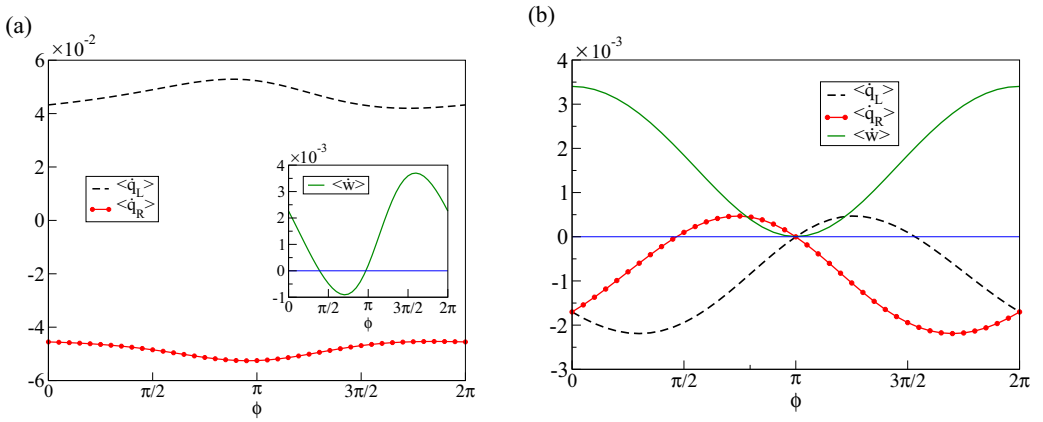

FIG. 2. (a) Engine mode of operation. $\langle \dot{q}_L \rangle > 0$, $\langle \dot{q}_R \rangle < 0$ and $\langle \dot{w} \rangle < 0$ for certain values of the phase ϕ. Parameter values are $h_0 = 0.25$, $\tau = 190$, $T_L = 1.0$, $T_R = 0.1$. At $\phi = 0.7\pi$, maximum work is extracted from the system (inset). In all the results discussed further these parameters are considered to be optimal for engine mode of operation. (b) Pump-refrigerator mode of operation. Parameter values are $h_0 = 0.25$, $\tau = 225$, $T_L = 0.5$, $T_R = 0.5$. See, for example, at $\phi = 0.7\pi$, we have $\langle \dot{q}_R \rangle > 0$, $\langle \dot{w} \rangle > 0$, and $\langle \dot{q}_L \rangle < 0$ implying heat is taken from the right bath, work is done on the system, and heat is dissipated into the left bath. In all the results discussed further, these parameters are considered to be optimal for pump-refrigerator mode of operation. Zero line is just a guide for the eyes. See Ref. [25] for details.

Since each spin is in contact with a separate heat bath, the spin flip rates themselves can be used to evaluate flip probabilities by multiplying them with the time step dt. In general, flip rates need not be smaller than 1, thus we choose the rate constant r such that this problem does not arise [27]. At each step, if a spin flips, heat is exchanged between the left (right) spin and left (right) bath. We calculate these rates of heat exchange, the rate of work done on the first and second spin in the steady state, over one time period.

For our systems, there are four thermodynamically possible machines which are engine, heaters 1 and 2, and refrigerator [13]. The actual mode of operation is determined by signs of heat exchanges $\langle \dot{q}_L \rangle$, $\langle \dot{q}_R \rangle$ and the total work done $\langle \dot{w} \rangle$. For $T_L \geqslant T_R$, these modes of operation are described as:

(1) Engine mode: $\langle \dot{q}_L \rangle > 0$, $\langle \dot{q}_R \rangle < 0$, $\langle \dot{w} \rangle < 0$, implying heat flows from left bath into the system, which is used by the working substance to do work on the external agent and remaining heat is dissipated into the right bath.

(2) Heater 1 mode: $\langle \dot{q}_L \rangle < 0$, $\langle \dot{q}_R \rangle < 0$, $\langle \dot{w} \rangle > 0$. In this case external agent delivers large amount of heat in form of work into system and this heat is then dissipated in both left and right reservoirs.

(3) Heater 2 mode: $\langle \dot{q}_L \rangle > 0$, $\langle \dot{q}_R \rangle < 0$, $\langle \dot{w} \rangle > 0$ heat flows from the left bath, as well as work is done on the system, hence a large amount of heat is dissipated in the right bath.

(4) Refrigerator mode: $\langle \dot{q}_L \rangle < 0$, $\langle \dot{q}_R \rangle > 0$, $\langle \dot{w} \rangle > 0$, heat is taken from the right bath which is at a slightly lower temperature than the left bath, work is done on the system and this results in transfer of heat to the left bath.

In our model the phase difference ϕ and the time period τ alone can determine different modes of operations as can be seen from Figs. 2(a), 2(b) and Fig. 3(a), 3(b).

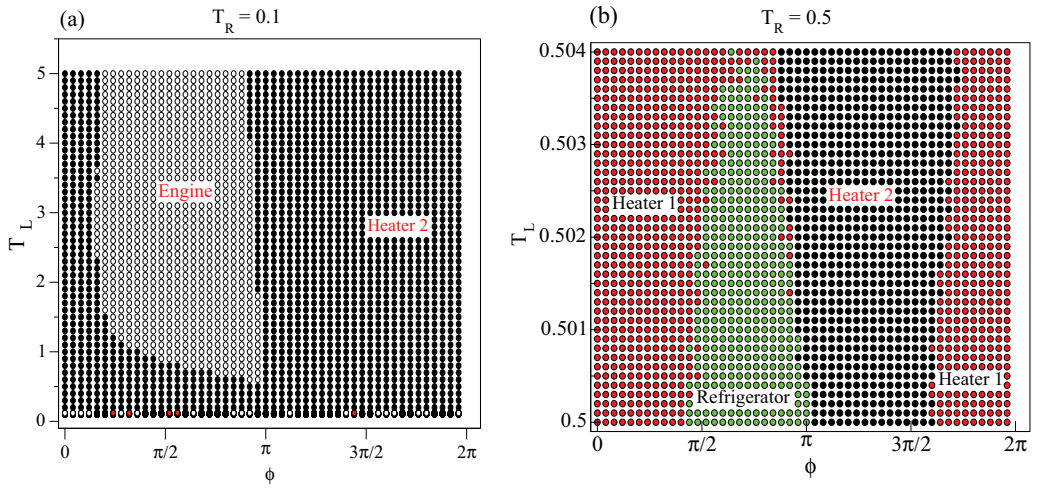

FIG. 3. (a) Shows the phase diagram as a function of the phase difference ϕ for engine mode of operation. Black solid circles indicate Heater 2 mode and open black circles indicate engine mode. (b) Phase diagram for the refrigerator mode. Solid red circles heater 1 (for $0 \leqslant \phi < \pi/2$ and $3\pi/2 < \phi \leqslant 2\pi$) and solid green circles refrigerator (for $\pi/2 \leqslant \phi < \pi$), solid black circles heater 2 mode (for $\pi \leqslant \phi < 3\pi/2$). Different modes are also indicated in the figure.

We are also interested in studying fluctuations in heat exchanged and work done as well as to study how sensitive is the performance of the model in engine and pump-refrigerator mode, on the optimal parameter values described above. Hence, we construct phase diagram for both modes of operations as a function of the phase ϕ and the temperature T_L keeping $T_R = 0.1$ for engine mode and $T_R = 0.5$ for pump mode of operation. These phase diagrams are shown in Figs. 3(a) and 3(b), respectively. Figure 3(a) shows how engine mode of operation depends on the phase ϕ and the temperature T_L for fixed $T_R = 0.1$ and $\tau = 190$. It has two distinct domains namely engine and heater 2. For $\pi/4 < \phi < \pi$ and $T_L - T_R > 1$, engine behavior is observed ($\langle \dot{q}_L \rangle > 0$, $\langle \dot{q}_R \rangle < 0$, $\langle \dot{w} \rangle < 0$). Other part of the diagram is dominated by heater 2 operation. In Fig. 3(b), we plot phase diagram for the refrigerator mode of operation where $T_R = 0.5$, $\tau = 225$. It is equally dominated by heater 1, refrigerator, and heater 2 modes with refrigerator mode occurring in a narrow strip between $\pi/2 < \phi < \pi$, and for very small temperature differences $T_L - T_R \leqslant 0.005$.

We now examine how different modes of operations depend on different parameters in the model other than the phase ϕ. To this end we construct the phase diagram where we keep the phase $\phi = 0.7\pi$, temperature $T_R = 0.1$ fixed, and vary T_L for different time periods of driving τ. This phase diagram is shown in Fig. 4(a). We see that for small $\tau \sim 50$, work done $\langle \dot{w} \rangle < 0$ with $\langle \dot{q}_L \rangle > 0$, $\langle \dot{q}_R \rangle < 0$, system works as an engine independent of the temperature difference $T_L - T_R$. For large $\tau > 50$ engine behavior persists but only for the moderate temperature differences $T_L - T_R \sim 1$. Other part of the phase diagram is mainly dominated by the heater 2 mode of operation where $\langle \dot{q}_L \rangle > 0$, $\langle \dot{q}_R \rangle < 0$, $\langle \dot{w} \rangle > 0$. After determining the phase diagram we choose optimal parameters and find the probability distribution of efficiency $P(\epsilon)$. This distribution is shown in Fig. 4(b). We see that the distribution is quite broad and has long power law tails [inset of Fig. 4(b)]. We would like to point out that in the quasistatic limit $\tau > 100$ distribution becomes more and more peaked and tails become shorter. But for small $\tau \sim 10$ tails of the distribution are long with power law decay.

Similar to engine mode of operation discussed above we also look at the pump-refrigerator mode. In this case we keep phase $\phi = 0.7\pi$, $T_R = 0.5$ fixed, and change T_L for different values of the time period τ. This phase diagram is presented in Fig. 4(c). Refrigerator mode ($\langle \dot{q}_L \rangle < 0$, $\langle \dot{q}_R \rangle > 0$, $\langle \dot{w} \rangle > 0$)

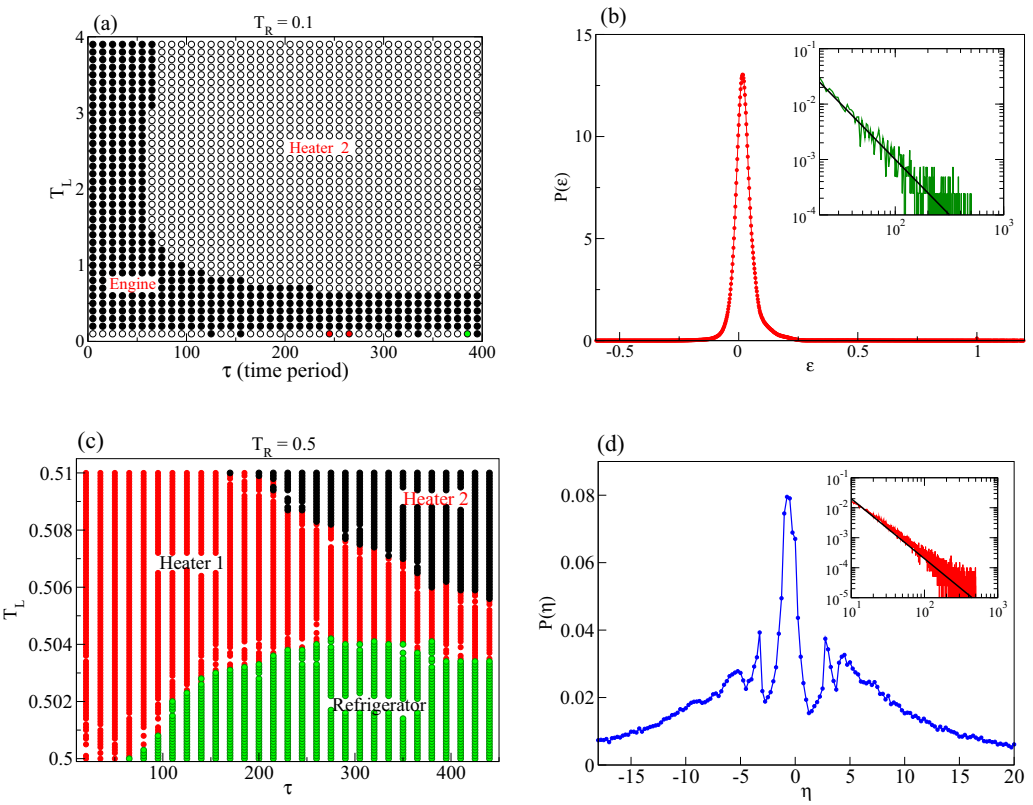

FIG. 4. (a) Phase diagram for Engine mode of operation. Here $T_R = 0.1$, $\phi = 0.7\pi$, $h_0 = 0.25$, and $J = 1.0$. Black solid circles represent engine operation while black open circles heater 2 operation. These modes are also indicated in the figure. (b) Distribution $P(\epsilon)$ of efficiency ϵ in the engine mode of operation, parameters used are $T_L = 1.0$, $T_R = 0.1$, $\phi = 0.7\pi$, $h_0 = 0.25$, and $\tau = 190$. Inset shows the tail part of the distribution for $\tau = 10$. Tail of the distribution can be fitted to a power law $a\epsilon^{-\alpha}$ with exponent close to 2 (solid black line). (c) Phase diagram for refrigerator mode of operation. Parameters are $T_R = 0.5$, $\phi = 0.7\pi$, $h_0 = 0.25$. Red portion (middle portion) shows heater 1 operation, while Black portion represents heater 2 operation (upper right part), and green refrigerator operation (bottom right part) is indicated in the figure. For refrigerator mode of operation one requires the temperature difference between T_L and T_R to be small. (d) Distribution $P(\eta)$ of coefficient of performance η in the refrigerator mode of operation. Parameters used are $T_L = 0.5$, $T_R = 0.5$, $\phi = 0.7\pi$, $h_0 = 0.25$, and $\tau = 225$. Inset shows the tail part of the distribution. Tail of the distribution can again be fitted to a power law $b\eta^{-\alpha}$ with exponent close to 2 (solid black line).

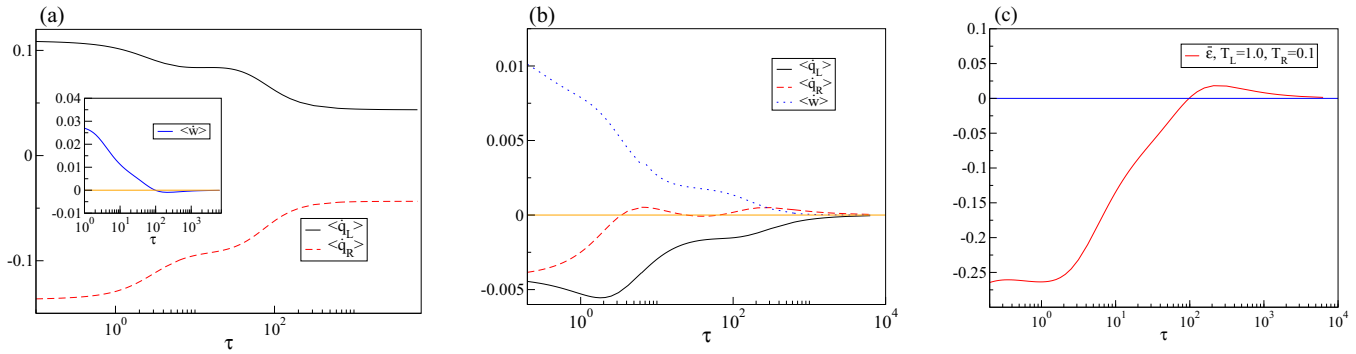

FIG. 5. Plot of $\langle \dot{q}_L \rangle$, $\langle \dot{q}_R \rangle$, $\langle \dot{w} \rangle$ as a function of time period of external driving τ in different modes of operation. Here $h_0 = 0.25$, $\phi = 0.7\pi$. (a) Engine mode, $T_L = 1.0$, $T_R = 0.1$. (b) Refrigerator mode, $T_L = 0.5$, $T_R = 0.5$. (c) Efficiency $\bar{\epsilon}$ as a function of time period of external driving τ in engine mode, $T_L = 1.0$, $T_R = 0.1$. Zero line is just a guide for the eyes.

occurs in a thin band for $\tau \geqslant 100$ for temperature differences $T_L - T_R \sim 0.005$. Other regions of the phase diagram are namely dominated by heater 1 ($\langle \dot{q}_L \rangle < 0$, $\langle \dot{q}_R \rangle < 0$, $\langle \dot{w} \rangle > 0$), for $\tau < 100$ and $T_L - T_R > 0.005$. Heater 2 mode ($\langle \dot{q}_L \rangle > 0$, $\langle \dot{q}_R \rangle < 0$, $\langle \dot{w} \rangle > 0$) appears for larger values of $\tau > 200$ and larger temperature differences. We also plot the distribution of COP $P(\eta)$ in Fig. 4(d). We see that distribution is broad with many distinct minima and long power law tails [inset Fig. 4(b)] with exponent ~ -2.

We also look at the behavior of different average heat currents namely $\langle \dot{q}_L \rangle$, $\langle \dot{q}_R \rangle$, $\langle \dot{w} \rangle$, as a function of the driving period τ. This is crucial in order to understand how this engine performs when compared to the Carnot engine. In Fig. 5(a), we plot these currents for the engine mode, where as expected $\langle \dot{q}_L \rangle > 0$, $\langle \dot{q}_R \rangle < 0$ for all τ values, and they saturate to some finite value in the quasistatic limit $\tau \to \infty$. However, work done is negative only for a short interval when $\tau \sim 100$ [inset of Fig. 5(a)]. Figure 5(b) shows the refrigerator mode where behavior changes from heater 1 for $\tau \sim 10$ to refrigerator ($\tau \sim 50$) and then to heater 1 for $\tau \sim 100$. Refrigerator mode recurs for $\tau \sim 500$ before all heat currents vanish in the quasistatic limit. Last, in Fig. 5(c) we plot average efficiency $\bar{\epsilon}$ as a function of τ where for $\tau < 100$ system is in the heater 2 mode ($\langle \dot{q}_L \rangle > 0$, $\langle \dot{q}_R \rangle < 0$, $\langle \dot{w} \rangle > 0$ [see Fig. 5(a)], reaches a maximum value $\bar{\epsilon} \sim 0.025$ at $\tau \sim 190$, and then vanishes as $\tau \to \infty$, in quasistatic limit. This is consistent with the fact that though $\langle \dot{q}_L \rangle$ is finite at large τ[see Fig. 5(a)], work done actually approaches zero in the quasistatic limit [inset of 5(a)]. This behavior is absent in usual colloidal engines where efficiency actually approaches Carnot efficiency in the quasistatic limit, distinguishing our model from earlier models [13,14]. Finally, in Fig. 6 we plot power $\langle \dot{w} \rangle / \tau$, as a function of the time period τ for fixed T_L, T_R, and ϕ. As expected, for $\tau \sim 1$ finite amount of power is generated but it approaches zero as τ is increased.

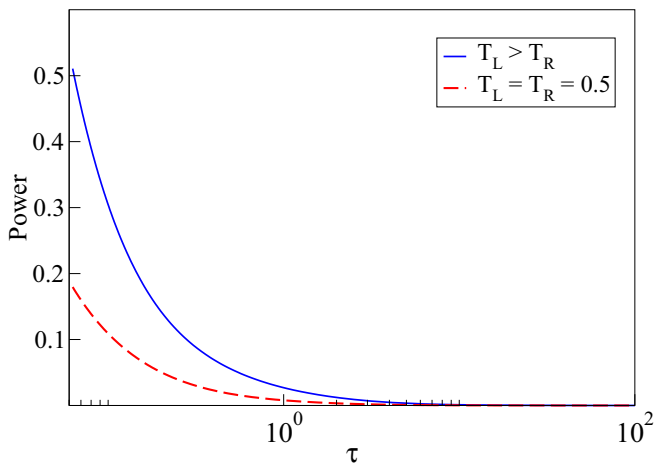

FIG. 6. Plot of Power generated namely $\langle \dot{w} \rangle / \tau$ as a function of time period of external driving τ. For two sets of parameters $h_0 = 0.25$, $\phi = 0.7\pi$, $T_L = 1.0$, $T_R = 0.1$ and $T_L = 0.5$, $T_R = 0.5$.

IV. CONCLUSION

To conclude we have studied a model of two classical Ising spin interacting simultaneously with two heat baths and driven by time dependent, phase different magnetic fields. Unlike earlier models, the working substance is in contact with heat baths for the full duration of the driving protocol. We also found that the performance of the system as an engine or a pump is highly affected by thermal fluctuations. For usual heat engines, e.g., colloidal particles in contact with multiple baths, one expects that the efficiency should approach Carnot limit $1 - T_c/T_h$ in the quasistatic or under zero power generation limit [4]. Since our model is in contact with both heat baths simultaneously, efficiency never reaches the Carnot limit due to nonzero entropy production, even in the quasistatic limit. This is consistent with the Büttiker-Landauer model [28–31]. This nonzero entropy production rate defined as $\langle \dot{S} \rangle = \langle -(\dot{q}_L/T_L) - (\dot{q}_R/T_R) \rangle$, can be seen from Fig. 5(a), where $\langle \dot{q}_L \rangle$, $\langle \dot{q}_R \rangle$ are nonzero in the quasistatic case. In fact, in our model the efficiency goes to zero as the time period $\tau \to \infty$ as seen Fig. 5(c). We also point out that when the limit of small temperature difference and small driving frequency is taken simultaneously, the efficiency still remains much smaller than the Carnot efficiency. Similarly, the COP is much smaller than the Carnot bound for the same reason. Reliability of the engine is an important technological issue. Here reliability implies for how many cycles out of the total cycles, over which the averages are calculated, the device actually performed as an engine. We found that for optimal parameters in engine mode

of operation with $\tau = 190$ the reliability was about 75%. It was also seen that for $\tau \sim 10$ reliability was about 35%. As the time period increased ($\tau \sim 2000$), reliability almost reached 100%, showing similar behavior as that of macroscopic engines. COP also shows similar behavior. This again points to the fact that fluctuations largely affect the performance. One interesting issue would be to look for possible ways to optimize the power and efficiency, on which we are currently working. To quantify fluctuations more concretely, we also numerically obtained probability distribution functions for efficiency $P(\epsilon)$ and COP $P(\eta)$. We found distributions to be very broad with power law tails, with exponent ~ -2. This points to the fact that fluctuations about the mean are much larger than unity. Currently we are studying the possibilities of an optimal protocol to increase the reliability of the engine, which may be independent of the time period.

ACKNOWLEDGMENTS

R.M. thanks Department of Science and Technology (DST), India for financial support. D.B., J.N., and R.M. thank the IIT Delhi HPC facility for computational resources. A.M.J. also thanks DST, India for support through a J. C. Bose National Fellowship. Authors thank Varsha Banerjee for careful reading of the manuscript. We also thank the referees for making many valuable suggestions toward the improvement of this manuscript.

[1] R. Feynman, R. Leighton, and M. Sands, *The Feynman Lectures on Physics* (Addison-Wesley, Reading, MA, 1966), Vol. 1, Chap. 46.
[2] E. Roldan, I. A. Martinez, J. M. R. Parrondo, and D. Petrov, Nat. Phys. **10**, 457 (2014).
[3] S. Toyabe, T. Sagawa, M. Ueda, E. Muneyuki, and M. Sano, Nat. Phys. **6**, 988 (2010).
[4] I. A. Martínez, É. Roldán, L. Dinis, and R. A. Rica, Soft Matter **13**, 22 (2017).
[5] S. Krishnamurthy, S. Ghosh, D. Chatterji, R. Ganapathy, and A. K. Sood, Nat. Phys. **12**, 1134 (2016).
[6] C. Bustamante, J. Liphardt, and F. Ritort, Phys. Today **58**, 43 (2005).
[7] S. Lahiri, S. Rana, and A. M. Jayannavar, J. Phys. A **45**, 465001 (2012).
[8] H. B. Callen, *Introduction to Thermodynamics and Thermostatistics* (John Wiley and Sons, New York, 1985).
[9] K. Sekimoto, J. Phys. Soc. Jpn. **66**, 1234 (1997).
[10] K. Sekimoto, Prog. Theor. Phys. Suppl. **130**, 17 (1998).
[11] K. Sekimoto, *Stochastic Energetics* (Springer, Heidelberg, 2010).
[12] P. S. Pal, A. Saha, and A. M. Jayannavar, Int. J. Mod. Phys. B **30**, 1650219 (2016).
[13] S. Rana, P. S. Pal, A. Saha, and A. M. Jayannavar, Physica A **444**, 783 (2016).
[14] S. Rana, P. S. Pal, Arnab Saha, and A. M. Jayannavar, Phys. Rev. E **90**, 042146 (2014).
[15] M. C. Mahato, T. P. Pareek, and A. M. Jayannavar, Int. J. Mod. Phys. B **10**, 3857 (1996).
[16] Z. C. Tu, Phys. Rev. E **89**, 052148 (2014).
[17] V. Holubec, J. Stat. Mech. (2014) P05022.
[18] U. Seifert, Rep. Prog. Phys. **75**, 126001 (2012).
[19] C. Van den Broeck and R. Kawai, Phys. Rev. Lett. **96**, 210601 (2006).
[20] G. Verley, T. Willaert, C. Van den Broeck, and M. Esposito, Nat. Commun. **5**, 4721 (2014).
[21] H. Qian, S. Saffarian, and E. L. Elson, Proc. Natl. Acad. Sci. USA **99**, 10376 (2002).
[22] K. H. Kim and H. Qian, Phys. Rev. Lett. **93**, 120602 (2004).
[23] M. L. Rosinberg, T. Munakata, and G. Tarjus, Phys. Rev. E **91**, 042114 (2015).
[24] A. Saha, R. Marathe, and A. M. Jayannavar, arXiv:1609.03459 (2016).
[25] R. Marathe, A. M. Jayannavar, and A. Dhar, Phy. Rev. E **75**, 030103(R) (2007).
[26] R. J. Glauber, J. Math. Phys. **4**, 294 (1963).
[27] V. Holubec *et al.*, Europhys. Lett. **93**, 40003 (2011).
[28] M. Z. Büttiker, Phys. B - Condens. Matter **68**, 161 (1987).
[29] R. J. Landauer, J. Stat. Phys. **53**, 233 (1988).
[30] R. Benjamin and R. Kawai, Phys. Rev. E **77**, 051132 (2008).
[31] R. Benjamin, Int. J. Mod. Phys. B **28**, 1450055 (2014).